Rapid #: -16309954

CROSS REF ID: **3463010**

LENDER: **AZU :: Main Library**

BORROWER: **GZM :: Memorial Library**

TYPE:	Article CC:CCL
JOURNAL TITLE:	Radiology
USER JOURNAL TITLE:	Radiology
ARTICLE TITLE:	Transstenotic pressure gradients: measurement in swine--retrospectively ECG-gated 3D phase-contrast MR angiography versus endovascular pressure-sensing guidewires
ARTICLE AUTHOR:	Lum, Darren P
VOLUME:	245
ISSUE:	3
MONTH:	
YEAR:	2007
PAGES:	751-760
ISSN:	0033-8419
OCLC #:	

Processed by RapidX: 6/26/2020 4:54:43 PM

Transstenotic Pressure Gradients: Measurement in Swine—Retrospectively ECG-gated 3D Phase-Contrast MR Angiography versus Endovascular Pressure-sensing Guidewires[1]

Darren P. Lum, MD
Kevin M. Johnson, BS
Russell K. Paul, MD
Aquilla S. Turk, DO
Daniel W. Consigny, BA, RT(R)
Julie R. Grinde, BS
Charles A. Mistretta, PhD
Thomas M. Grist, MD

Purpose: To prospectively evaluate the hypothesis that retrospectively electrocardiographically gated phase contrast with vastly undersampled isotropic projection reconstruction (VIPR) magnetic resonance (MR) angiography data sets can be used to measure transstenotic pressure gradients (TSPGs) in vivo.

Materials and Methods: TSPGs were calculated by using phase-contrast VIPR MR angiography data sets; measurements obtained with a pair of endovascular pressure-sensing guidewires served as a reference standard. With institutional animal care and use committee approval, 12 swine underwent surgical creation of stenoses at the left common carotid, right renal, and left external iliac arteries. The percentage stenosis and reference diameter of the lesions were calculated from conventional digital subtraction angiograms. A pair of 0.014-inch pressure-sensing guidewires was placed in tandem; sensors 1 cm distal and 1 cm proximal to the lesions measured the mean TSPG. Phase-contrast VIPR phase difference images were analyzed with an iterative technique based on the Navier-Stokes equations to determine the mean TSPG. Pearson product correlation was calculated, and Bland-Altman plots were generated to determine the degree of agreement between the two methods.

Results: Twenty-one lesions (12 carotid, nine iliac; mean percentage stenosis, 52.4%; range, 29.8%–64.9%; mean reference diameter, 3.4 mm; range, 2.4–5.6 mm) were analyzed. For carotid and iliac lesions, phase-contrast VIPR and guidewire TSPG measurements were highly correlated ($r = 0.952$, $P < .001$). Bland-Altman plots (bias, 0.86 mm Hg; limits of agreement: −6.17 to 7.88 mm Hg) showed good agreement. Measurements in renal lesions ($n = 9$) were poorly correlated ($r = -0.081$, $P = .835$) and were excluded because of image degradation secondary to respiratory motion.

Conclusion: Phase-contrast MR angiography with VIPR enables reliable measurements of TSPG in carotid and iliac lesions that are comparable to those obtained with endovascular pressure-sensing guidewires. However, further work to compensate for respiratory motion is required to extend this technique to the renal arteries.

[1] From the Department of Radiology, University of Wisconsin Hospital and Clinics, 600 Highland Ave, CSC E3/311, Madison, WI 53792. From the 2006 RSNA Annual Meeting. Received November 20, 2006; revision requested January 19, 2007; revision received January 31; accepted March 16; final version accepted May 11. Supported by National Institutes of Health grant R01HL072260-02 and a 2005-2006 Research Resident Grant from the RSNA Research and Education Foundation. **Address correspondence to** D.P.L. (e-mail: *lum@wisc.edu*).

The presence of transstenotic pressure gradients has been correlated with turbulent flow and intravoxel spin dephasing, as seen in conventional three-dimensional (3D) cartesian phase-contrast magnetic resonance (MR) angiography (1). In current clinical practice, the presence of this dephasing artifact is often used to assist in grading the hemodynamic significance of a renal artery lesion (2,3). Study results have shown that lesion morphology as determined with digital subtraction angiography (DSA) alone in moderate (50%–75%) stenosis is not an accurate indicator of hemodynamically significant lesions (4). The measurement of transstenotic pressure gradients in conjunction with DSA in moderate stenosis is helpful in guiding pretherapeutic decision making in renal (5) and iliac (4,6) lesions. Methods of calculating transstenotic pressure gradients from time-resolved 3D phase-contrast MR angiography data by using the Navier-Stokes equations have been demonstrated (7), but have yet to become widely adopted in clinical practice. Obstacles to clinical acceptance include lengthy imaging times, trade-offs in sequence design that sacrifice high spatial resolution, and the lack of commercial workstations to perform the required image postprocessing and calculations.

A technique for phase contrast with vastly undersampled isotropic projection reconstruction (VIPR) has been developed (8). Advantages of phase-contrast VIPR include broader spatial coverage, isotropic spatial resolution, and smaller voxel sizes than those at conventional 3D cartesian phase-contrast imaging. Undersampling the periphery of k-space allows dramatic reductions in imaging time without compromising broad volumetric coverage or high spatial resolution. Radial streak artifacts introduced with undersampling are minimized in phase-contrast imaging because of the subtraction of stationary tissues during image reconstruction. Less spin dephasing has been observed around turbulent flow with phase-contrast VIPR, likely because of smaller voxel sizes. A retrospectively electrocardiographically (ECG)-gated phase-contrast VIPR sequence yields four-dimensional (time-varying 3D) velocity vector fields, enabling quantitative flow analysis at vascular stenoses.

Thus, the purpose of our study was to prospectively evaluate our hypothesis that retrospectively ECG-gated phase-contrast VIPR MR angiography data sets can be used to measure transstenotic pressure gradients in vivo.

Advances in Knowledge

- The high spatial resolution of phase-contrast vastly undersampled isotropic projection reconstruction (VIPR) allows for quantitative flow analysis in vessels as small as 3 mm in diameter.
- Retrospectively electrocardiographically gated phase-contrast VIPR MR angiography provides reliable measurements of transstenotic pressure gradients at mild to moderate carotid and iliac stenoses; measurements are comparable to those obtained with a pair of endovascular pressure-sensing guidewires (Pearson product correlation: $r = 0.952$, $P < .001$; Bland-Altman analysis: bias = 0.86 mm Hg, limits of agreement = −6.17 to 7.88 mm Hg).

Materials and Methods

The endovascular pressure-sensing guidewires and interface units used in this study were provided by RADI Medical Systems, Uppsala, Sweden. None of the authors is an employee of or a consultant for this company. The authors were aware of industry support and had full control of the data and information included in this study.

Animals

Between October 27, 2005, and February 8, 2006, studies were conducted with prior approval from our institution's animal care and use committee. These studies were performed with the supervision of a trained surgeon (D.W.C., with 4 years of experience) and fully conformed to the National Institutes of Health guidelines for use of laboratory animals. Twelve crossbred juvenile swine from a commercial vendor (Arlington Farms, Arlington, Wis; mean weight, 79.4 lb [35.73 kg]) underwent surgical placement of artificial stenoses at the left common carotid, right renal, and left external iliac arteries. General endotracheal anesthesia was induced after sedation and analgesia with 2.2 mg xylazine hydrochloride (Rompun; Bayer HealthCare, Leverkusen, Germany) per kilogram of body weight and 7 mg/kg tiletamine HCl/zolazepam HCl (Telazol; Fort Dodge Animal Health, Fort Dodge, Iowa). Anesthesia was maintained with 1%–3% isoflurane (Phoenix Pharmaceutical, St Joseph, Mo) throughout the entire procedure. Each study typically

Implication for Patient Care

- Retrospectively electrocardiographically gated phase-contrast vastly undersampled isotropic projection reconstruction MR angiography can potentially provide a noninvasive method for inferring the hemodynamic significance of a vascular lesion by estimating the transstenotic pressure gradient.

Published online
10.1148/radiol.2453061946

Radiology 2007; 245:751–760

Abbreviations:
CI = confidence interval
DSA = digital subtraction angiography
ECG = electrocardiography
3D = three-dimensional
VIPR = vastly undersampled isotropic projection reconstruction

Author contributions:
Guarantors of integrity of entire study, D.P.L., T.M.G.; study concepts/study design or data acquisition or data analysis/interpretation, all authors; manuscript drafting or manuscript revision for important intellectual content, all authors; manuscript final version approval, all authors; literature research, D.P.L., K.M.J., A.S.T.; experimental studies, D.P.L., K.M.J., R.K.P., A.S.T., D.W.C., J.R.G., T.M.G.; statistical analysis, D.P.L., T.M.G.; and manuscript editing, all authors

See Materials and Methods for pertinent disclosures.

See also Science to Practice in this issue.

required 7–8 hours of anesthesia and entailed the surgical creation of artificial stenoses, endovascular pressure gradient measurements, MR imaging, and DSA to document lesion morphology. After each study, the animal was euthanized by means of intravenous injection of a minimum of 0.2 mL of a solution containing pentobarbital sodium (390 mg/mL) and phenytoin sodium (50 mg/mL) (Beuthanasia-D; Schering-Plough Animal Health, Union, NJ) per kilogram of body weight.

Surgery

A 4-F right internal jugular vein sheath was placed for MR imaging contrast material injections. A 6-F sheath was placed at the right femoral artery for angiography and endovascular pressure measurements. After surgical exposure, 3-mm-wide plastic cable ties were placed at the left common carotid, right renal, and left external iliac arteries and tightened manually (all procedures were performed by D.W.C. and J.R.G.). A mobile fluoroscopic C-arm (OEC 9800; GE Healthcare Technologies, Waukesha, Wis) was used for guidance. A 100-cm-long 5-F angled catheter (Torcon NB Advantage DAV; Cook, Bloomington, Ind) was used for selective angiography to place the cable ties and adjust the severity of stenosis. To prevent the formation of thrombus around the stenoses, 1000 U of heparin was administered per hour.

Reference Standard Endovascular Pressure Measurements

All endovascular transstenotic pressure measurements were performed with a pair of 200-cm-long 0.014-inch pressure-sensing guidewires (PressureWire 4; RADI Medical Systems) that were connected to interface units (RADI Pressure Wire Interface Unit). Each interface unit was connected to an analog-to-digital converter (U12; Labjack, Lakewood, Colo), which was then connected to a standard laptop personal computer running Windows XP (Microsoft, Redmond, Wash) and data acquisition software (Labview, version 7; National Instruments, Austin, Tex).

The heart rate of the animal was recorded (J.R.G.) immediately prior to the endovascular measurements. Both wires were placed at the surgical tabletop at the same height and were calibrated in their packaging coil after flushing with 20 mL normal saline. After calibration and zeroing of the patient-monitoring system (D.P.L.), the wires were introduced into a dual-headed rotating hemostatic valve (Duostat; Guidant, Santa Clara, Calif) connected to the 100-cm 5-F angled catheter.

After the catheter was introduced into the 6-F right femoral sheath, selective "road map" angiograms of each lesion were obtained. Once the pressure-sensing wires were positioned across the stenosis, the guiding catheter was retracted out of the vessel so as to prevent alteration of flow. A standard United States coin (a dime) was used for distance calibration (J.R.G.). The pressure sensor was located 3 cm from the end of the radioopaque platinum-tipped guidewire. The sensors were placed 1 cm proximal and 1 cm distal to the center of the stenosis (D.W.C., R.K.P., A.S.T.). Approximately 60 seconds were allowed to elapse, permitting flow across the stenosis to equilibrate. Digital pressure waveforms proximal and distal to the lesion were then simultaneously recorded with the analog-to-digital converter. The mean gradient was recorded as the difference between the mean pressure readings from the two wires (D.P.L., K.M.J.). Gradients were rounded to the nearest whole number value in millimeters of mercury. Once measurements were made at all three vessel beds, the catheter and wires were removed before MR imaging.

MR Imaging

All MR imaging examinations were performed with a 1.5-T system (Signa EXCITE HD Twinspeed, version 12; GE Healthcare) with an eight-channel phased-array body coil (GE Healthcare). Conventional 3D gadolinium-enhanced MR angiography (Table 1) was performed in each vessel bed to define the lesion location and orientation. The renal and iliac arteries were visualized in the same coronal acquisition after the power injection (Spectris Solaris; Medrad, Indianola, Pa) of 0.2 mmol/kg contrast material (gadodiamide, Omniscan; GE Healthcare) at 1 mL/sec. A separate acquisition and injection of contrast material (gadodiamide) at 1 mL/sec was used to visualize the carotid arteries. Flow measurements were performed orthogonal to the vessel (examination prescription and monitoring, D.P.L.) both proximal and distal to the lesion with a standard ECG-gated two-dimensional phase-contrast sequence with velocity encoding set at 100 and 150 cm/sec (Table 1). These flow measurements were performed to select the optimal velocity encoding for subsequent phase-contrast VIPR examinations so that velocity aliasing was avoided.

A phase-contrast VIPR examination (Table 1), with flow encoded by using the same velocity encoding in all three flow directions, was performed at each lesion after the power injection (Spectris Solaris) of 0.2 mmol/kg contrast material (gadodiamide) at 1 mL/sec. All examinations started approximately 30 seconds after the contrast material injection was complete, taking advantage of the additional signal provided by contrast material circulating within the blood pool. All phase-contrast VIPR examinations were performed during breathing that was controlled by a mechanical ventilator, without respiratory gating. The heart rate of the animal was recorded (D.P.L.) at the beginning of the phase-contrast VIPR sequence for each vessel territory. The average acquisition time for phase-contrast VIPR examinations was 668 seconds ± 3 (standard deviation) (ie, 11 minutes 8 seconds); acquisition time ranged between 664 and 677 seconds.

DSA Technique

After the MR imaging examination, reference DSA was performed (Innova 4100; GE Healthcare) to document lesion morphology (D.W.C., R.K.P., D.P.L.). The 100-cm 5-F angled catheter was used to select each vessel bed. The carotid stenosis was imaged in the anteroposterior and lateral projections at a contrast material injection rate of 1.5 mL/sec. Renal lesions were imaged with 25° caudal and 25° cranial projections

Table 1

MR Imaging Sequence Parameters

Parameter	Three-dimensional Gadolinium-enhanced MR Angiography	ECG-gated Two-dimensional Cine Phase-contrast MR Imaging	ECG-gated Phase-Contrast MR Imaging with VIPR
Repetition time (msec)	3.1	9.9	9.8
Echo time (msec)	0.9	4.4	4.1
Velocity encoding (cm/sec)	NA	100 And 150	Variable (70–175)
Flip angle (degrees)	30	45	20
Bandwidth (kHz)	62.5	15.625	31.25
Field of view (cm)	32	20	30
Matrix size	256 × 256	256 × 128	384 × 384
No. of sections	48	20 Cardiac phases	384
Section thickness (mm)	2.0	5.0	0.78
Coverage (cm)	9.6 (Anteroposterior, y-axis)	NA	14.4 (Superoinferior, z-axis)
Voxel volume (mm^3)	3.125	6.1	0.477
No. of projections	NA	NA	17 000
Acquisition length (sec)	22	22–36 (Depending on heart rate)	664–677
Gradient mode and strength	"Zoom" mode; 40 mT/m gradient strength, 150 mT/m/msec slew rate	"Zoom" mode; 40 mT/m gradient strength, 150 mT/m/msec slew rate	Whole-body mode; 23 mT/m gradient strength, 80 mT/m/msec slew rate
Comments	Reconstruction with zero-filled interpolation to 512 × 512 image matrix; phase field of view, 80%; turbo mode; elliptical centric; 70% partial Fourier encoding in section direction	Phase field of view, 80%; number of signals acquired, 1.0; views per segment, two	

Note.—NA = not applicable.

at a contrast material injection rate of 1.5 mL/sec. Each iliac stenosis was imaged in the 20° right anterior oblique and 20° left anterior oblique projections at a contrast material injection rate of 2 mL/sec. All DSA images were obtained at 7.5 frames per second at a 16-cm field of view (matrix, 800 × 800). The contrast material used was iohexol (Omnipaque 350 [350 milligrams of iodine per milliliter]; GE Healthcare) diluted as 50 mL contrast material with 100 mL normal saline and injected through a power injector (Liebel-Flarsheim Angiomat Illumena; Mallinckrodt, Cincinnati, Ohio).

The frame of maximal opacification was analyzed (D.P.L.) at an image analysis workstation (Cardiac X-Ray Applications: Stenosis Analysis, version 1.2, algorithm 4.0.12, Advantage Windows software version 4.2_04; GE Healthcare) to determine the lesion percentage stenosis and reference diameter. The reference location for the stenosis analysis was placed either proximal or distal to the stenosis at the most normal-appearing segment (9). For each lesion, the percentage stenosis and reference diameter are reported as the average result of two views.

MR Angiography–derived Transstenotic Pressure Gradients

Phase-contrast VIPR MR images were reconstructed by using the complex difference algorithm for morphologic analysis. Phase difference processing was also performed in all three flow directions by using a view-sharing method for data at the periphery of k-space and

Figure 1

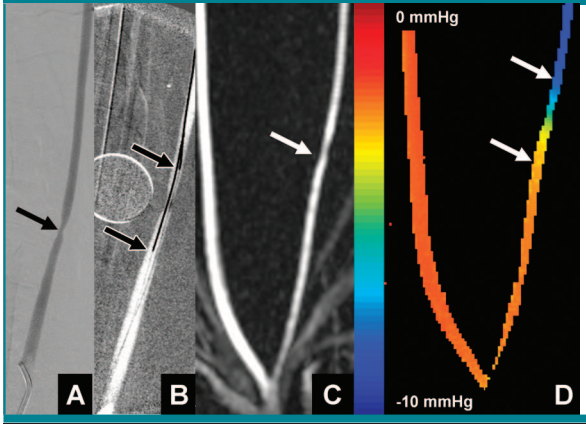

Figure 1: Stenosis at left common carotid artery. *A,* DSA image in anteroposterior projection shows 46.4% diameter stenosis (reference diameter, 2.6 mm) (arrow). *B,* "Road map" angiogram obtained during endovascular pressure gradient measurements. Two 0.014-inch guidewires were placed in tandem. Pressure sensors (arrows) located 1 cm proximal and 1 cm distal to center of stenosis measured a 6–mm Hg pressure gradient. *C,* Subvolume coronal maximum intensity projection of complex difference phase-contrast VIPR MR angiography data (repetition time msec/echo time msec, 9.8/4.1; flip angle, 20°; velocity encoding, 120 cm/sec; 0.78-mm isotropic spatial resolution). Image was reconstructed from all projections collected during entire acquisition and shows average flow. Arrow = stenosis. *D,* Pressure map derived from phase-contrast VIPR phase difference data. Arrows show start and end locations, corresponding to 1 cm proximal and 1 cm distal to center of stenosis, from which pressure gradient was calculated. A 7 mm Hg pressure gradient was calculated at this lesion.

Figure 2

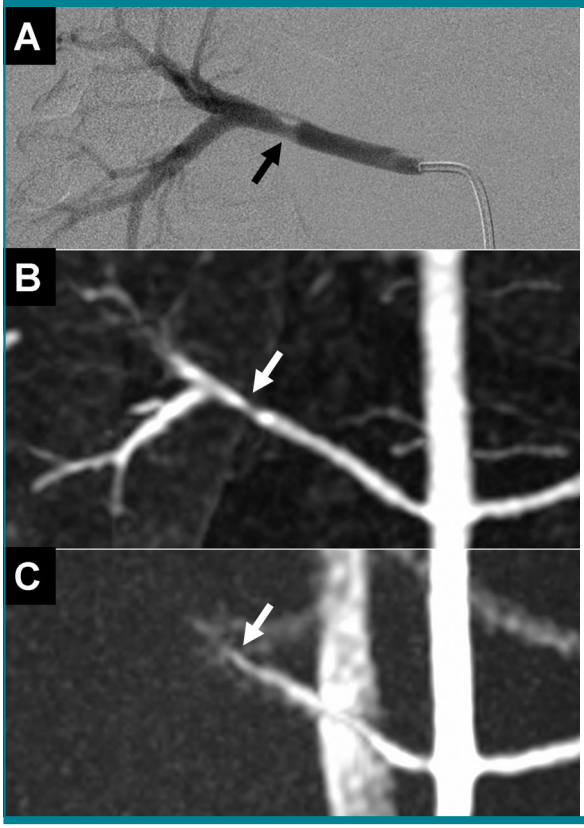

Figure 2: Stenosis at right renal artery. *A,* DSA image in 25° caudal projection shows 38.7% diameter stenosis (reference diameter, 3.4 mm) (arrow). A 28 mm Hg gradient was measured with endovascular guidewires. *B,* Subvolume coronal maximum intensity projection reconstruction of conventional 3D gadolinium-enhanced MR angiography data (3.1/0.9; flip angle, 30°) shows stenosis (arrow). *C,* Subvolume coronal maximum intensity projection of complex difference phase-contrast VIPR MR angiography data (9.8/4.1; flip angle, 20°; velocity encoding, 120 cm/sec; 0.78-mm isotropic spatial resolution). Image was reconstructed from all projections collected during entire acquisition and shows average flow. Poor flow distal to stenosis (arrow) is visualized. Nonvisualization of flow distal to the stenosis is believed to be related to respiratory motion. Blurring associated with respiratory motion prevents accurate measurement of the pressure gradient in the renal arteries.

Figure 3

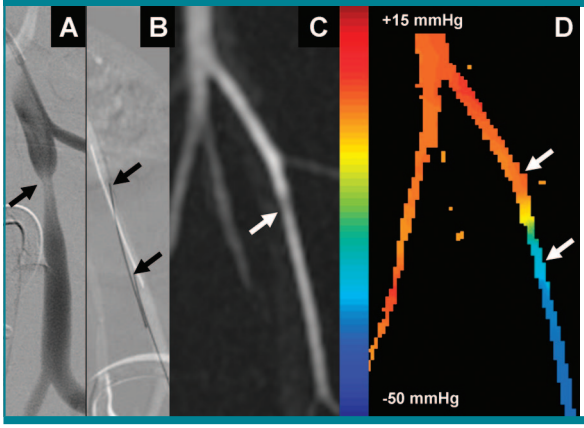

Figure 3: Stenosis at left external iliac artery. *A,* DSA image in 20° left anterior oblique projection shows 61.5% diameter stenosis (reference diameter, 3.9 mm) (arrow). *B,* "Road map" angiogram obtained during endovascular pressure gradient measurement. Two 0.014-inch guidewires were placed in tandem. Pressure sensors (arrows) located 1 cm proximal and 1 cm distal to center of stenosis measured a 23 mm Hg pressure gradient. *C,* Subvolume coronal maximum intensity projection of complex difference phase-contrast VIPR MR angiography data (9.8/4.1; flip angle, 20°; velocity encoding, 125 cm/sec; 0.78-mm isotropic spatial resolution). Image was reconstructed from all projections collected during entire acquisition and shows average flow. Arrow = stenosis. *D,* Pressure map derived from phase-contrast VIPR phase difference data. Arrows show start and end locations, corresponding to 1 cm proximal and 1 cm distal to center of stenosis, from which pressure gradient was calculated. A 28 mm Hg pressure gradient was calculated at this lesion.

a "tornado" filter, as described by Barger et al (10). At each vessel bed, 15–20 cardiac phases were typically reconstructed. For each projection angle, the time required to accomplish flow encoding in all three directions was four excitations (four times the repetition time). Accounting for the view sharing described above, the temporal resolution of the sequence depended on the spatial frequency and smoothly varied from four times the repetition time at the center of k-space to 12 times the repetition time at the edge of k-space (Table 1). With a repetition time of 9.8 msec, the temporal resolution of the reconstructed images ranged from 39.2 msec for the image contrast within the vessels (center of k-space) to 117.6 msec for the edge information in the images (periphery of k-space).

All calculations were performed by the same observer (K.M.J.), who was blinded to the endovascular pressure

gradient results at the time of MR imaging data analysis. Pressure gradients were calculated with software (Matlab; MathWorks, Natick, Mass) by using the Navier-Stokes equations and an iterative algorithm previously validated in phantom models (7,11,13). The pressure gradients were calculated by using a four-step process of vessel segmentation, pressure gradient determination, integrative pressure determination, and iterative refinement. A user-set threshold was applied for vessel segmentation, followed by an antiisland filter for vessel wall smoothing and removal of isolated regions. Central difference equations were then employed to determine the pressure gradients, with corrections for errors occurring at the vessel edges. A seed point method was used to determine an initial pressure map, which was then iteratively refined by using a path-averaging algorithm (7). Finally, dynamic pressure maps were averaged, and the mean pressure gradient was then measured 1 cm proximal and 1 cm distal to the center of the stenosis. All pressure gradient values were rounded to the nearest whole number value in millimeters of mercury.

Statistical Analysis

All data are presented as means ± standard deviations. Scatterplots of the MR imaging–derived pressure gradients versus the guidewire-measured pressure gradients for individual vascular territories were generated. Pearson product correlations, along with 95% confidence intervals (CIs), were calculated separately for each vessel territory and were tested for significance by using the Fisher Z transformation (D.P.L.). The difference between the correlations was tested after the Fisher Z transformation. Transstenotic pressure gradients obtained from phase-contrast VIPR MR angiography data were then compared with those recorded by using the endovascular guidewires. The agreement between the two measurement techniques was assessed (D.P.L., T.M.G.) by using the method of Bland and Altman (14). P values of less than .05 were considered to indicate statistically significant differences. Statistical analysis and plot gen-

Figure 4

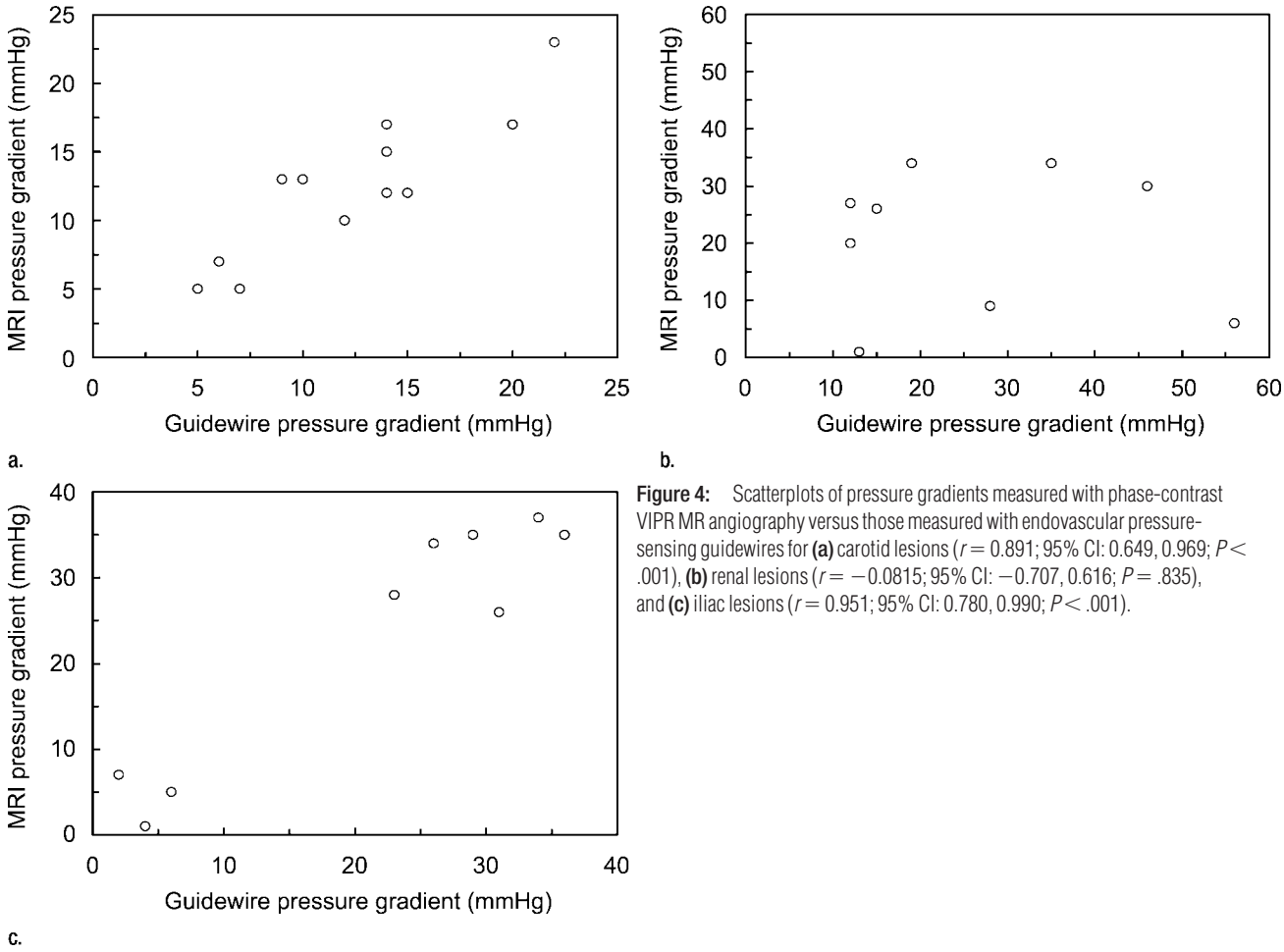

Figure 4: Scatterplots of pressure gradients measured with phase-contrast VIPR MR angiography versus those measured with endovascular pressure-sensing guidewires for **(a)** carotid lesions ($r = 0.891$; 95% CI: 0.649, 0.969; $P < .001$), **(b)** renal lesions ($r = -0.0815$; 95% CI: −0.707, 0.616; $P = .835$), and **(c)** iliac lesions ($r = 0.951$; 95% CI: 0.780, 0.990; $P < .001$).

eration were performed by using software (Matlab).

Results

Transstenotic pressure gradients from 12 carotid lesions, nine renal lesions, and nine iliac lesions were analyzed (Figs 1–3). Data were not available for two iliac lesions because of MR imaging prescription error, while another iliac lesion could not be examined because of complete vascular occlusion. Three renal lesions could not be evaluated secondary to nonvisualization of flow distal to the stenosis. Scatterplots for each vessel territory showed that there were significant correlations for both carotid (Fig 4a) and iliac (Fig 4c) lesions. The correlation coefficients for the two territories were compared after the Fisher Z transformation and were not significantly different ($P = .427$). Pressure gradient measurements for the nine renal lesions (Fig 4b) were poorly correlated ($r = -0.081$, $P = .835$) and were excluded from further analysis.

The percentage diameter stenosis (Table 2) spanned a clinically significant range (29.8%–64.9%) of values; a range of both large and small pressure gradients were measured with the endovascular wires (2–36 mm Hg). Vessel diameters ranged from 2.4 to 5.6 mm. Pressure maps (D in Figs 1–3) depicted the transstenotic pressure gradients in representative carotid and iliac lesions. The variability in heart rate (Table 2) between endovascular and MR imaging pressure measurements indicated that these paired pressure gradient measurements were not always obtained in identical hemodynamic states. Despite these differences, very high correlation was found between the transstenotic pressure gradients obtained with the endovascular wires and those obtained with phase-contrast VIPR MR angiography (Fig 5a). Bland-Altman plots (Fig 5b) showed good agreement between the two techniques.

Table 2

Characteristics of Carotid and Iliac Stenotic Lesions

Vessel Territory and Mean Percentage Stenosis at DSA	Mean Reference Diameter (mm)	Guidewire Measurement of Mean Pressure Gradient (mm Hg)	Mean Pressure Gradient at MR Angiography (mm Hg)	Heart Rate during Guidewire Measurement (beats/min)	Heart Rate during MR Angiography (beats/min)
Carotid					
51.0	4.0	22	23	102	98
48.8	2.7	12	10	100	117
46.4	2.6	6	7	97	96
52.9	3.9	9	13	86	108
53.3	3.3	20	17	92	80
52.0	3.2	14	15	126	105
49.2	2.8	14	17	100	103
41.4	3.3	15	12	116	150
64.9	3.7	7	5	107	105
55.2	3.6	5	5	87	85
52.5	2.6	14	12	78	88
55.0	2.4	10	13	109	120
Iliac					
61.5	3.9	23	28	102	101
62.0	3.3	2	7	97	99
58.5	3.6	26	34	86	98
56.8	3.4	31	26	92	75
50.6	4.5	36	35	126	110
55.2	3.7	29	35	100	85
54.5	4.5	6	5	116	130
49.0	5.6	4	1	87	80
29.8	2.5	34	37	78	80
Overall*					
52.4 ± 7.5	3.4 ± 0.8	16.1 ± 10.4	17.0 ± 11.4	99.2 ± 13.8	100.6 ± 18.4

* Data are mean values ± standard deviations.

Discussion

In vascular territories with little motion, such as the carotid and iliac arteries, our results demonstrated high correlation and good agreement between the two measurement techniques. However, in vessels affected by respiratory motion, such as the renal arteries, the correlation between the two techniques was poor. Because of factors associated with surgical exposure, the artificial renal lesions were located at the distal renal artery and hence were subject to larger excursions associated with respiratory motion. This raises the question of whether the accuracy of phase-contrast VIPR pressure gradients would be improved in ostial renal artery lesions. In light of the promising results in vascular territories with little motion, further work is underway to extend this technique for intraabdominal and intrathoracic applications.

Measurement of transstenotic pressure gradients has been shown to be useful for guiding decision making in endovascular therapy for renal and iliac lesions. The Dutch Iliac Stent Trial Study Group investigators treated 100 iliac lesions with percutaneous transluminal angioplasty (6). A stent was placed after angioplasty if a residual mean intraarterial pressure gradient of greater than 10 mm Hg was measured. These researchers concluded that the decision to deploy an iliac stent after angioplasty should be based on the residual transstenotic pressure gradient and not on lesion morphology after angioplasty. Several more recent studies have involved investigation of the use of endovascular pressure-sensing guidewires to measure transstenotic pressure gradients (15–17) and fractional flow reserve (18) in renal artery lesions. Poor correlation between the pressure gradient

and the severity of stenosis was found in several of these studies (16–18). Taking into account the finding of poor agreement among three radiologists regarding the morphologic severity of renal artery lesions in the Dutch Renal Artery Stenosis Intervention Cooperative study (19), it would be prudent that some measure of the physiologic significance of a lesion, in addition to stenosis morphology, be considered before endovascular therapy.

With respect to carotid lesions, measurement of transstenotic pressure gradients is not typically performed in clinical practice. Efforts are made to minimize crossing a lesion before therapy because of the risks of downstream embolization. Published indications for carotid artery angioplasty and stent placement (20) describe symptomatic patients with severe diameter stenosis (as defined by the North American Symptomatic Carotid Endarterectomy Trial measurement criteria [21]) of 70% or greater as candidates for endovascular therapy. As our data demonstrate, lesions with moderate stenosis (50%–75%) may result in transstenotic pressure gradients greater than 10 mm Hg. The severity of a carotid lesion is inferred with Doppler ultrasonography in current clinical practice (22). Noninvasive estimation of transstenotic pressure gradients with retrospectively ECG-gated phase-contrast MR angiography is a potentially powerful tool, providing another objective measure for grading the hemodynamic significance of a stenotic vascular lesion.

In vitro measurement of transstenotic pressure gradients with phase-contrast VIPR MR angiography has been validated in phantom models with a flow pump (23). Initial in vivo work has been performed in which phase-contrast VIPR–derived pressure gradients in a canine carotid stenosis model were correlated with microcatheter pressure readings as a standard of reference (24). Colyer et al (16) have shown that a 0.014-inch endovascular pressure-sensing guidewire yields more accurate pressure gradient measurements than do catheter-based techniques. Because the presence of a catheter across a lesion can reduce the stenosis cross section, we simultaneously measured the transstenotic pressure gradient with a pair of 0.014-inch guidewires.

Time-resolved phase-contrast techniques have been previously reported (25–29) and have primarily been applied toward the visualization of blood flow patterns. These techniques have been studied for the evaluation of intracardiac flow (30,31) and pressure (32), as well as for flow analysis within large vessels such as the thoracic aorta (27,28,33). The VIPR sampling strategy enables high-spatial-resolution flow imaging in small vessels in a nonprohibitive imaging time. The technique reported by Markl and colleagues (33) for in vivo studies of the thoracic aorta required an imaging time of 14.8–22.6 minutes, yielding a temporal resolution of 76.7–80.7 msec, a spatial resolution of 1.17 × 1.56 × 2.60 mm, and volumetric coverage of 30 × 22.5 × 8.3 cm. In comparison, the phase-contrast VIPR sequence in our study yielded broader volumetric coverage (30 × 30 × 14.4 cm), submillimeter isotropic resolution (0.78 × 0.78 × 0.78 mm), and comparable temporal resolution (39.2 msec for the image contrast, 117.6 msec for edge information). However, the faster phase-contrast VIPR acquisition time (approximately 11 minutes) was likely related to the fact that we did not utilize respiratory compensation. Nasiraei-Moghaddam et al (12) ex-

Figure 5

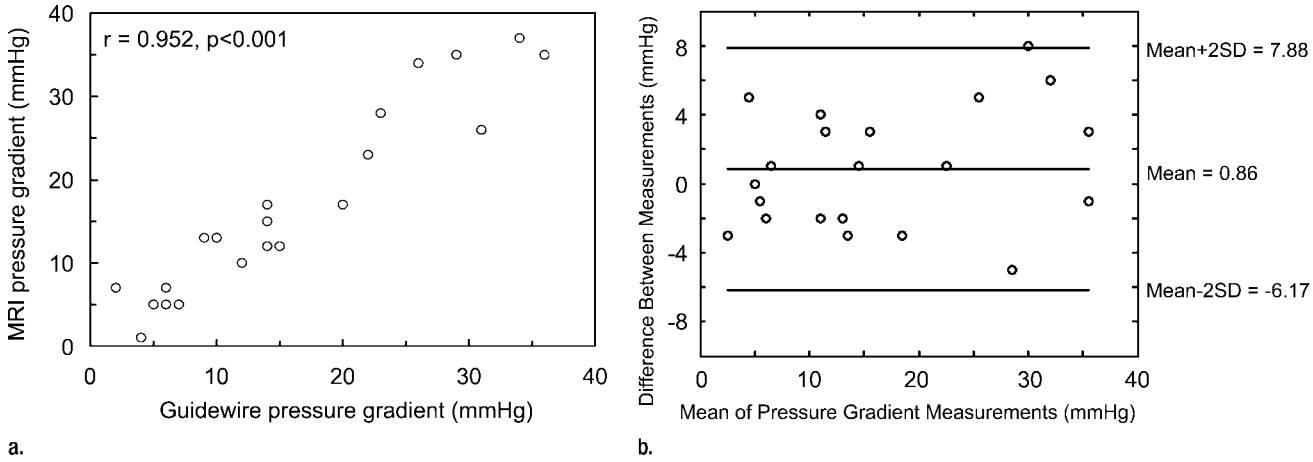

Figure 5: Graphs of data in carotid and iliac lesions combined ($n = 21$). **(a)** Scatterplot of pressure gradients measured with phase-contrast VIPR MR angiography versus those measured with endovascular pressure-sensing guidewires ($r = 0.952$; 95% CI: 0.884, 0.981; $P < .001$). **(b)** Bland-Altman plot shows degree of agreement between pressure gradients measured with phase-contrast VIPR MR angiography and those measured with endovascular pressure-sensing guidewires. Central line demonstrates bias; outer lines demonstrate upper and lower limits of agreement (±2 standard deviations *[SD]*). Bias in estimation of pressure gradients between the two techniques is small (0.86 mm Hg; 95% CI: −0.74, 2.46 mm Hg), with a standard deviation of 3.51. The limits of agreement between the two measurement techniques are narrow (−6.17 to 7.88 mm Hg), indicating a high degree of agreement.

plored the calculation of transstenotic pressure gradients with the Navier-Stokes equations in axisymmetric phantom models of vascular stenosis. The submillimeter isotropic spatial resolution of phase-contrast VIPR directly addresses their finding that high spatial resolution is critical for creating accurate pressure maps in poststenotic turbulent flow.

Further technical developments to reduce acquisition time may include extension of a two-dimensional radial trajectory (34) into three dimensions (35,36), highly constrained back-projection reconstruction (37), or the use of parallel imaging (38). Meanwhile, sampling the center of k-space in VIPR with each excitation makes compensation for subject translational or rotational motion possible (39). In order to extend phase-contrast VIPR into vessel territories affected by respiration, topics rich for exploration include motion correction, respiratory triggering, and imaging time reduction.

Empiric selection of the velocity encoded is not robust and is prone to operator error. Automated selection of the optimal velocity encoding for the lesion of interest, such as with the prescan described by Ringgaard et al (40), would be useful. Furthermore, a variable (40–42) or multiple (43,44) velocity-encoding acquisition could enable better characterization of both slow flow (ie, flow distal to severe stenosis) and rapid flow (ie, poststenotic jets), while still avoiding velocity aliasing.

The amount of data to be analyzed with four-dimensional (time-resolved 3D) phase-contrast techniques can be unwieldy. For each cardiac phase, four volumes (complex difference and phase difference for each of three flow directions) are reconstructed. Each lesion in our study resulted in the reconstruction of $4N\ 384 \times 384 \times 384$ volumes of data, where N is the number of cardiac phases. Pressure gradient analysis of this data in Matlab is time consuming and labor intensive. Semiautomatic software for pressure gradient analysis from four-dimensional phase-contrast data would be valuable and would contribute to the reproducibility of pressure gradient measurements.

Our study had limitations. Endovascular measurements and MR imaging examinations were not performed simultaneously in identical conditions. During endovascular measurements, both wires crossed the lesion, while MR imaging was performed in the absence of wires. Because of the logistic constraints, transportation, MR imaging setup, and anatomy of interest localization, 2–3 hours typically elapsed between endovascular and MR imaging–based pressure gradient measurements. We did not record mean arterial pressure because our arterial pressure transducer is not MR imaging compatible. However, the heart rate was recorded at the start of each pressure gradient measurement, demonstrating the variability in the hemodynamic state between measurements. Furthermore, the time between endovascular gradient measurements and DSA for documentation of stenosis morphology was up to 5 hours. Factors such as vasospasm between the times of endovascular gradient measurement, MR angiography, and DSA cannot be accounted for.

The contour of the artificial lesions studied was smooth and tapering; additional studies are in progress to validate our method in actual atherosclerotic lesions. Finally, further work is required to demonstrate the clinical utility of phase-contrast VIPR. Whether phase-contrast VIPR transstenotic pressure gradient measurements improve the detection of hemodynamically significant lesions compared with conventional 3D cartesian phase-contrast MR angiography is a subject of continued investigation.

Practical applications: Retrospectively ECG-gated phase-contrast VIPR provided reliable measurements of transstenotic pressure gradients in our sample of mild to moderate carotid and iliac stenoses. Unfortunately, we were not successful in evaluating vessels affected by respiratory motion, such as stenotic renal arteries. Further work accounting for respiratory motion is under way to improve this technique for intraabdominal and intrathoracic applications. For carotid and iliac lesions, measurements were comparable to those obtained with a pair of endovascular pressure-sensing guidewires over a wide range of gradients in vessels as small as 3 mm in diameter. This technique holds potential to more accurately characterize the hemodynamic significance of a lesion, thus expanding the prognostic capabilities of MR imaging. This could affect the care of patients by guiding decisions regarding therapeutic endovascular intervention with an initial noninvasive imaging examination.

Acknowledgments: The authors thank RADI Medical Systems for loaning the pressure interface units and for providing the pressure-sensing guidewires utilized for this study. The authors thank Kelli Hellenbrand, Nathan Frey, and Wendy Trotter for their assistance in performing the MR imaging examinations; Jason Scott, Mike McArdle, Blake White, Patty Ryan-Meyer, and Patty Crane for their assistance in performing the angiographic examinations; and Frank Korosec, PhD, and Oliver Wieben, PhD, for many helpful and thoughtful discussions.

References

1. Mustert BR, Williams DM, Prince MR. In vitro model of arterial stenosis: correlation of MR signal dephasing and trans-stenotic pressure gradients. Magn Reson Imaging 1998;16:301–310.
2. Prince MR, Schoenberg SO, Ward JS, Londy FJ, Wakefield TW, Stanley JC. Hemodynamically significant atherosclerotic renal artery stenosis: MR angiographic features. Radiology 1997;205:128–136.
3. Wasser MN, Westenberg J, van der Hulst VP, et al. Hemodynamic significance of renal artery stenosis: digital subtraction angiography versus systolically gated three-dimensional phase-contrast MR angiography. Radiology 1997;202:333–338.
4. Udoff EJ, Barth KH, Harrington DP, Kaufman SL, White RI. Hemodynamic significance of iliac artery stenosis: pressure measurements during angiography. Radiology 1979;132:289–293.
5. Martin LG, Rundback JH, Sacks D, et al. Quality improvement guidelines for angiography, angioplasty, and stent placement in the diagnosis and treatment of renal artery stenosis in adults. J Vasc Interv Radiol 2002;13:1069–1083.
6. Tetteroo E, van Engelen AD, Spithoven JH, Tielbeek AV, van der Graaf Y, Mali WP. Stent placement after iliac angioplasty: comparison of hemodynamic and angiographic criteria. Dutch Iliac Stent Trial Study Group. Radiology 1996;201:155–159.

7. Tyszka JM, Laidlaw DH, Asa JW, Silverman JM. Three-dimensional, time-resolved (4D) relative pressure mapping using magnetic resonance imaging. J Magn Reson Imaging 2000; 12:321–329.
8. Gu T, Korosec FR, Block WF, et al. PC VIPR: a high-speed 3D phase-contrast method for flow quantification and high-resolution angiography. AJNR Am J Neuroradiol 2005;26:743–749.
9. Ota H, Takase K, Rikimaru H, et al. Quantitative vascular measurements in arterial occlusive disease. RadioGraphics 2005;25: 1141–1158.
10. Barger AV, Block WF, Toropov Y, Grist TM, Mistretta CA. Time-resolved contrast-enhanced imaging with isotropic resolution and broad coverage using an undersampled 3D projection trajectory. Magn Reson Med 2002;48:297–305.
11. Yang GZ, Kilner PJ, Wood NB, Underwood SR, Firmin DN. Computation of flow pressure fields from magnetic resonance velocity mapping. Magn Reson Med 1996; 36:520–526.
12. Nasiraei-Moghaddam A, Behrens G, Fatouraee N, Agarwal R, Choi ET, Amini AA. Factors affecting the accuracy of pressure measurements in vascular stenoses from phase-contrast MRI. Magn Reson Med 2004;52:300–309.
13. Thompson RB, McVeigh ER. Fast measurement of intracardiac pressure differences with 2D breath-hold phase-contrast MRI. Magn Reson Med 2003;49:1056–1066.
14. Bland JM, Altman DG. Statistical methods for assessing agreement between two methods of clinical measurement. Lancet 1986;1:307–310.
15. Gross CM, Kramer J, Weingartner O, et al. Determination of renal arterial stenosis severity: comparison of pressure gradient and vessel diameter. Radiology 2001; 220:751–756.
16. Colyer WR Jr, Cooper CJ, Burket MW, Thomas WJ. Utility of a 0.014" pressure-sensing guidewire to assess renal artery translesional systolic pressure gradients. Catheter Cardiovasc Interv 2003;59:372–377.
17. Jones NJ, Bates ER, Chetcuti SJ, Lederman RJ, Grossman PM. Usefulness of translesional pressure gradient and pharmacological provocation for the assessment of intermediate renal artery disease. Catheter Cardiovasc Interv 2006;68:429–434.
18. Subramanian R, White CJ, Rosenfield K, et al. Renal fractional flow reserve: a hemodynamic evaluation of moderate renal artery stenoses. Catheter Cardiovasc Interv 2005;64:480–486.
19. van Jaarsveld BC, Pieterman H, van Dijk LC, et al. Inter-observer variability in the angiographic assessment of renal artery stenosis. DRASTIC study group. Dutch Renal Artery Stenosis Intervention Cooperative. J Hypertens 1999;17:1731–1736.
20. Barr JD, Connors JJ 3rd, Sacks D, et al. Quality improvement guidelines for the performance of cervical carotid angioplasty and stent placement. AJNR Am J Neuroradiol 2003;24:2020–2034.
21. Beneficial effect of carotid endarterectomy in symptomatic patients with high-grade carotid stenosis. North American Symptomatic Carotid Endarterectomy Trial Collaborators. N Engl J Med 1991;325:445–453.
22. Grant EG, Benson CB, Moneta GL, et al. Carotid artery stenosis: gray-scale and Doppler US diagnosis—Society of Radiologists in Ultrasound Consensus Conference. Radiology 2003;229:340–346.
23. Johnson KM, Gu T, Mistretta CA. 4D pressure mapping with time-resolved PC VIPR [abstr]. In: Proceedings of the Thirteenth Meeting of the International Society for Magnetic Resonance in Medicine. Berkeley, Calif: International Society for Magnetic Resonance in Medicine, 2005; 135.
24. Turk AS, Johnson KM, Lum D, et al. Physiologic and anatomic assessment of a canine carotid artery stenosis model utilizing phase contrast with vastly undersampled isotropic projection imaging. AJNR Am J Neuroradiol 2007;28:111–115.
25. Mohiaddin RH, Yang GZ, Kilner PJ. Visualization of flow by vector analysis of multidirectional cine MR velocity mapping. J Comput Assist Tomogr 1994;18:383–392.
26. Wigstrom L, Sjoqvist L, Wranne B. Temporally resolved 3D phase-contrast imaging. Magn Reson Med 1996;36:800–803.
27. Bogren HG, Buonocore MH. 4D magnetic resonance velocity mapping of blood flow patterns in the aorta in young vs. elderly normal subjects. J Magn Reson Imaging 1999;10:861–869.
28. Kozerke S, Hasenkam JM, Pedersen EM, Boesiger P. Visualization of flow patterns distal to aortic valve prostheses in humans using a fast approach for cine 3D velocity mapping. J Magn Reson Imaging 2001;13: 690–698.
29. Markl M, Chan FP, Alley MT, et al. Time-resolved three-dimensional phase-contrast MRI. J Magn Reson Imaging 2003;17:499–506.
30. Wigstrom L, Ebbers T, Fyrenius A, et al. Particle trace visualization of intracardiac flow using time-resolved 3D phase contrast MRI. Magn Reson Med 1999;41:793–799.
31. Fyrenius A, Wigstrom L, Ebbers T, Karlsson M, Engvall J, Bolger AF. Three dimensional flow in the human left atrium. Heart 2001;86: 448–455.
32. Ebbers T, Wigstrom L, Bolger AF, Engvall J, Karlsson M. Estimation of relative cardiovascular pressures using time-resolved three-dimensional phase contrast MRI. Magn Reson Med 2001;45:872–879.
33. Markl M, Draney MT, Hope MD, et al. Time-resolved 3-dimensional velocity mapping in the thoracic aorta: visualization of 3-directional blood flow patterns in healthy volunteers and patients. J Comput Assist Tomogr 2004;28:459–468.
34. Wentland AL, Korosec FR, Vigen KK, Wieben O, Fine JP, Grist TM. Cine flow measurements using phase contrast with undersampled projections: in vitro validation and preliminary results in vivo. J Magn Reson Imaging 2006;24:945–951.
35. Peters DC, Korosec FR, Grist TM, et al. Undersampled projection reconstruction applied to MR angiography. Magn Reson Med 2000;43:91–101.
36. Vigen KK, Peters DC, Grist TM, Block WF, Mistretta CA. Undersampled projection-reconstruction imaging for time-resolved contrast-enhanced imaging. Magn Reson Med 2000;43:170–176.
37. Mistretta CA, Wieben O, Velikina J, et al. Highly constrained backprojection for time-resolved MRI. Magn Reson Med 2006;55:30–40.
38. Samsonov AA, Block WF, Arunachalam A, Field AS. Advances in locally constrained k-space-based parallel MRI. Magn Reson Med 2006;55:431–438.
39. Welch EB, Rossman PJ, Felmlee JP, Manduca A. Self-navigated motion correction using moments of spatial projections in radial MRI. Magn Reson Med 2004;52: 337–345.
40. Ringgaard S, Oyre SA, Pedersen EM. Arterial MR imaging phase-contrast flow measurement: improvements with varying velocity sensitivity during cardiac cycle. Radiology 2004;232:289–294.
41. Buonocore MH. Blood flow measurement using variable velocity encoding in the RR interval. Magn Reson Med 1993;29:790–795.
42. Swan JS, Grist TM, Weber DM, Sproat IA, Wojtowycz MM. MR angiography of the pelvis with variable velocity encoding and a phased-array coil. Radiology 1994;190: 363–369.
43. Lee AT, Pike GB, Pelc NJ. Three-point phase-contrast velocity measurements with increased velocity-to-noise ratio. Magn Reson Med 1995;33:122–126.
44. Lamothe MJ, Rutt BK. Multistep phase difference phase contrast imaging. J Magn Reson Imaging 1997;7:838–842.